ACS APPLIED MATERIALS & INTERFACES
Research Article
www.acsami.org

Micropatterning for the Control of Surface Cavitation: Visualization through High-Speed Imaging

Valentina Belova-Magri,*[†] Adam Brotchie,[†] Carlos Cairós,[‡] Robert Mettin,*[‡] and Helmuth Möhwald[†]

[†]Max Planck Institute of Colloids and Interfaces, Am Mühlenberg 1, 14476 Potsdam, Germany
[‡]Drittes Physikalisches Institut, Georg-August-Universität, Friedrich-Hund-Platz 1, 37077 Göttingen, Germany

Supporting Information

ABSTRACT: For the first time, we apply a high-speed imaging technique to record the activity of acoustically driven cavitation bubbles (86 kHz) on micropatterned surfaces with hydrophobic and hydrophilic stripes. The width of the hydrophobic stripes lies between 3.5 and 115 μm. This work provides the first direct visualization of the preferential location of bubbles on the hydrophobic areas of the patterns. The results confirm our previous prediction that surface cavitation strongly depends on the surface energy of the irradiated substrate. The observations show a remarkable effect of the stripe width on the size, movement, growth, splitting, and multiplying of the bubbles. The high-speed imaging also reveals that there is a minimal width of the hydrophobic stripes that allows bubble attraction and formation. Our observations are supported by a theoretical approach based on the forces acting on the bubbles.

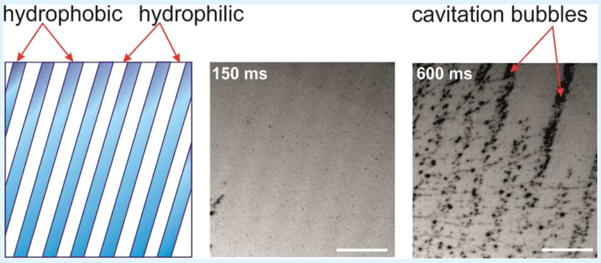

KEYWORDS: *ultrasound, surface cavitation, hydrophobic/hydrophilic surface, high-speed imaging, cavitation bubble, surface attached bubbles*

■ INTRODUCTION

Strong shear forces or ultrasound may produce gas bubbles in liquids, the collapse of which results in locally extreme physical (1×10^4 K, 1000 atm) and chemical (free-radical generation) conditions.[1−5] This, in turn, causes damage of materials, as has been known since a century ago for ship propellers,[6−8] but may also be exploited to construct new surfaces and imbue materials with desired functionalities.[9,10] To best make use of the process or to avoid erosion, it is necessary to measure and characterize the cavitation process. Bubble dynamics in acoustic fields spans a large range of time scales, from collapse phenomena below nanoseconds up to diffusion and translation effects taking place within milliseconds or beyond.[11] In particular bubble growth is a relatively slow process that is determined by gas diffusion but also significantly by collisions and mergers of many bubbles. Therefore, it is necessary to follow the movement and fate of many bubbles, which may occur on time scales of seconds. Because typical bubble dimensions are micrometers, high-speed optical microscopy has been employed as an ideal characterization method.[12−14]

Pioneering work to probe cavitation optically has been carried out by Lohse and co-workers,[15] who prepared hydrophobic wells on a surface where the bubbles were predictably nucleated, allowing the interactions between bubbles to be observed visually and described theoretically. However, in their work the cavitation bubbles were fixed at predefined nucleation sites, meaning that this method cannot be extended to observe the fate of moving bubbles. Overcoming this limitation, we have found that one can form tracks for bubbles on a surface, which can be achieved by using a striped surface pattern, and that by varying the stripe width, one may be able to estimate the forces pinning a bubble on a hydrophobic surface. One may also gain insight into the mechanism of gas transport near a surface needed to grow a bubble.

Herein, we introduce a method, which builds on previous work where we showed that cavitation bubbles, as theoretically expected, preferentially form on hydrophobic surfaces, where they caused damage to the surface.[16] In that study, however, it was not clear whether the bubbles formed at the surface escaped into the bulk. We now combine high-speed microscopy and chemical surface patterning to observe the growth, movement, and collision of acoustically excited bubbles on surfaces. We prove the existence of a lower limit of the hydrophobic stripe width for bubble attraction or formation and describe this with a simple theoretical model. An extension of this work to shorter time scales is expected to control collective cavitation events enabling the design of sophisticated surfaces. This could be used to prepare patterns of porous surfaces that contain a drug or other functional molecules in the vicinity of an untreated and hence flat surface.[17] Furthermore, surface modification under controlled cavitation for biomedical devices could significantly improve cell transportation and their adaptation to implanted materials.[18]

Received: November 17, 2014
Accepted: January 26, 2015
Published: January 26, 2015

DOI: 10.1021/am508062h
ACS Appl. Mater. Interfaces 2015, 7, 4100−4108

EXPERIMENTAL SECTION

The substrates used for our investigations were 10 mm × 20 mm plates cut from an optical quality Si wafer or a glass microscope slide sputter-coated with 40 nm of aluminum (Al). Polydimethylsiloxane (PDMS) replications of a Si master were used to transfer amphiphilic molecules (a mixture of octadecylphosphonic acid and octadecanethiol) to the substrate, which self-assemble as monolayers.[19] The patterned samples had six fields of different stripe dimensions in the range of 3.5 to 115 μm. The choice of the stripe widths was motivated by previous observations of differences in the response to ultrasonic irradiation at these dimensions.[20] The parameters of the samples are summarized in Table 1.

Table 1. Widths of the Hydrophobic and Hydrophilic Stripes in Micrometers of the Patterns Used To Optically Investigate the Surface Cavitation

	stripe width (μm)					
surface nature	I	II	III	IV	V	VI
hydrophobic	115	82	57	23	8.5	3.5
hydrophilic	120	90	60	35	14	8

The measured contact angle of the patterns is about 115−120°, depending on the width of the hydrophobic stripes. The bare Al is hydrophilic with a contact angle of 70°. Two types of substrate were used: chemically etched and nonetched patterns. The nonetched substrates had a height difference between the hydrophobic and hydrophilic stripes corresponding to the height of the amphiphilic molecules (ca. 3 nm). Etching was used to uniformly remove the upper Al layers and to improve the visual contrast between hydrophobic and hydrophilic areas of the patterns for the subsequent optical observation of cavitation. The height difference between the hydrophobic and hydrophilic areas of the etched pattern was about 20 nm, approximately 3 orders of magnitude smaller than the resonance bubble radius under the applied acoustic irradiation (about 35 μm at 86 kHz).[21] Therefore, the physical steps on the surface are not expected to influence the behavior of surface cavitation bubbles. A nonpatterned Si wafer was used as the control.

The experimental setup is presented in Figure 1. To observe the first moments of cavitation inception at the substrate surface, a high-speed camera (Fastcam APX RS, Photron Inc., U.S.A.) was mounted to a Nikon regular optical microscope (Microphot-FX, Nikon, Japan). The ultrasound cell, which comprised a glass Petri dish with a glued piezoceramic transducer to its underside, was mounted on the sample stage such that the affixed transducer fitted into the stage allowing the cell to sit flush. The position of the cell was adjusted using the clips on the stage. Inside the Petri dish, on the glass surface directly above the transducer, the substrate was adhered with double-sided tape (Tesa, 3M). The distance between the pattern and transducer was about 2 mm. The cell was filled to the top (filling height = cell height = 0.8 cm) with deionized water (k = 0.0005 mS/cm), and a glass cover slide was placed on the top, in contact with the water, to prevent oscillation of the interface. The experiments were conducted at room temperature and atmospheric pressure. The transducer was driven at a frequency of 86 kHz and a voltage of 30−60 V using a function generator (HP 33120A, Hewlett-Packard, U.S.A.) and a high speed bipolar power amplifier (HAS 4101, nF corp., Japan). In this configuration, the ultrasound waves propagate upward through the base of the cell. The sample was magnified with 5× and 10× Nikon objectives, and a Nikon Halogen 12 V 100 W lamp (Nikon, Japan) was used as the illumination source. The camera was set at either 5000, 10 000, or 100 000 frames per second (fps) on a continuous, manually end-triggered recording loop. Imaging was performed during the first few minutes of acoustic wave propagation.

RESULTS AND DISCUSSION

Figure 2 illustrates the cavitation bubble development on the nonetched pattern with different hydrophobic stripe widths of 115, 82, 23, and 8.5 μm. The pattern design is not detectable with a light microscope. For clarity it is sketched on the first frame. A simple alcohol−water exchange was performed to enrich the surface with gas. In brief, the substrate was covered with ethanol and subsequently flushed with an excess of deionized water. This procedure leads to the formation of gaseous domains such as nanobubbles and micropancakes, in particular at the hydrophobic regions.[22−24] Recently, we have shown that enrichment of the hydrophobic stripes with gas enhances cavitation events.[20] Hence, a high volume of adsorbed gas should amplify the number of cavitation bubbles at the surface.

High-speed imaging does not provide sufficient information about details of bubble nucleation but clearly shows for the first time that acoustic cavitation bubbles occupy only the hydro-

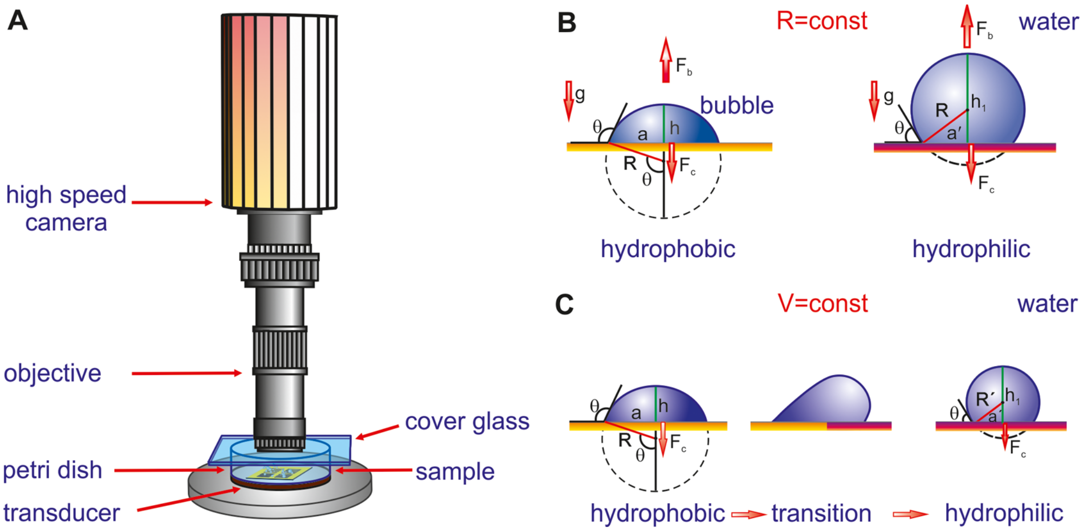

Figure 1. (A) Sketch of the experimental setup for visualizing the cavitation bubble behavior at the micropatterned surfaces in water. Imaging is done with a regular working microscope connected to a high-speed camera. (B) Side view of the forces acting on a cavitation bubble at hydrophobic and at hydrophilic surfaces. (C) Side view of the bubble that moves with a constant volume from the hydrophobic to the hydrophilic area. During its transition state, the bubble undergoes surface changes caused by its contact with the hydrophilic area.

DOI: 10.1021/am508062h
ACS Appl. Mater. Interfaces 2015, 7, 4100−4108

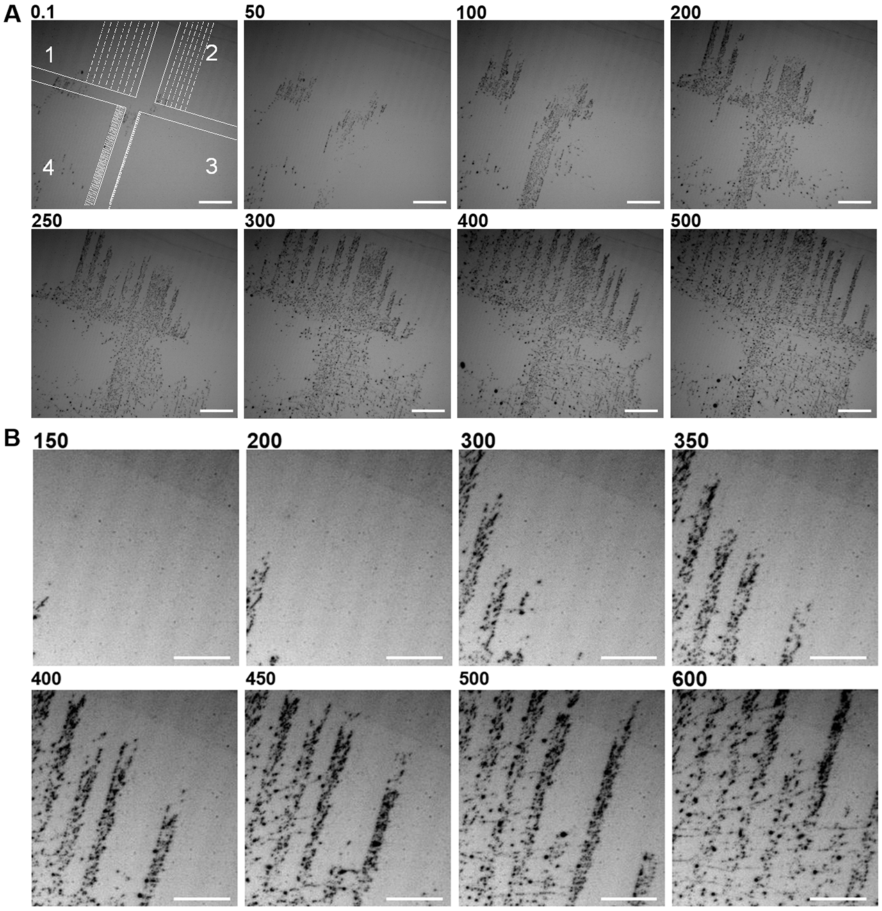

Figure 2. (A) Frames from sequences taken at 10 000 fps for investigation with a nonetched pattern containing four fields (denoted 1, 2, 3, 4) with different widths of the hydrophobic stripes (115, 82, 8.5, and 23 μm, respectively, clockwise from top left). The first frame shows an overlaid sketch with a pattern design. The scale bar is 500 μm. The numbers above the frames indicate the elapsed time in milliseconds after the start of acoustic irradiation. The movie is available in the Supporting Information (Movie S1). (B) The frames show the propagation of bubbles on the hydrophobic stripes of 82-μm width and their migration into the bulk. The scale bar is 300 μm, and numbers above frames again indicate the elapsed time in ms.

phobic areas of the patterns. This finding is in good agreement with our previous results which showed that a higher contact angle causes a lower nucleation energy barrier.[16] Thus, cavitation shows specificity for low-energy liquid/solid interfaces. It is interesting to note that surface cavitation is highly heterogeneous, occurring at some preferential sites and afterward spreading around the hydrophobic areas. We cannot determine from the movies if surface bubbles are actually nucleated at the hydrophobic surface, whether they nucleate elsewhere and move to the hydrophobic sites, or both. Once nucleated and attached, bubbles predominantly travel laterally, although they can also move from the surface into the bulk as can be clearly seen in Movie S1 (Supporting Information). The size of the hydrophobic area influences the cavitation bubble behavior: bubbles easily occupy the wider hydrophobic stripes (115 and 82 μm), where they move along the hydrophilic boundaries to progressively reach the central part of the stripes. On the contrary, slow bubble development is observed on the thinner stripes (23 and 8.5 μm). After 0.5 s of ultrasonic irradiation (Figure 2A, frame 500) the cavitation bubbles clearly follow the patterned structure of the sample. The close-up view of the patterned region with 82-μm hydrophobic stripes in Figure 2B allowed us to estimate the propagation velocity of the bubbles along the stripe. In all observed cases, this velocity is of the order of 5 mm/s. On the control sample we did not observe any attached bubbles.

Shifting the observation window to the narrow-striped region allowed us to detect the hydrophobic area where the surface bubbles do not grow or attach (Figure 3). Bubbles easily populate

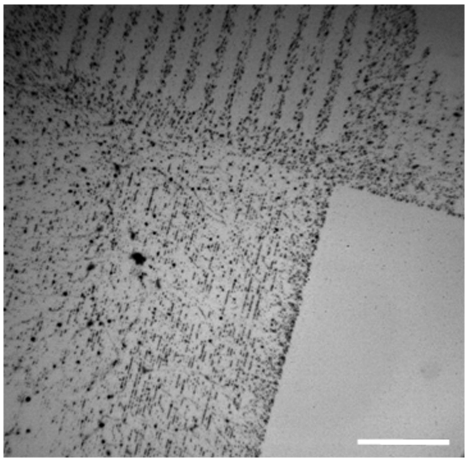

Figure 3. Frame from a sequence taken at 100 000 fps for a nonetched pattern containing four fields with different widths of hydrophobic stripes (82, 57, 3.5, and 8.5 μm, clockwise from top left). The scale bar is 500 μm. The elapsed time is 5.5 ms after the start of acoustic irradiation. This movie is available in the Supporting Information (Movie S1).

the areas with hydrophobic stripes of 8.5, 57, and 82 μm widths, while the area with narrow (3.5 μm) stripes remains devoid of visible bubbles. The stripe width is the only notable difference between these distinct areas of the pattern.

To summarize, we note the following key observations:

- For hydrophobic stripes with widths of 8.5 μm or greater, attached bubbles are observed only on these stripes and not between them.
- For stripe widths of 3.5 μm no attached bubbles are observed on the pattern.

To understand this, we would like to present in the following discussion some estimates of the forces acting on surface cavitation bubbles. We have previously estimated that the size of a critical nucleus is well below 1 μm and that the nucleation energy barrier is much lower on hydrophobic areas.[16] Hence one expects preferential nucleation on all hydrophobic stripes studied here irrespective of their widths. However, the question remains, up to which size a bubble would remain fixed on the stripes and how this depends on the contact angle (θ). We will consider bubbles with radii of curvature between 4 and 30 μm, as these are experimentally observed; for these bubbles the Laplace pressure due to surface tension, γ, can be neglected with respect to detachment.[25] We will later also show that Bjerknes forces, F_{Bj}, are negligible, and therefore, we can reduce the analysis to the balance of the capillary force, F_c, attracting the bubble to the surface and the buoyancy force, F_b, for our experimental geometry repelling it (as it directs upward). For a bubble with contact angle θ and radius of wall curvature R we derive the following, according to Jones et al.:[25]

$$F_c = 2\pi R\gamma \sin^2(\theta) \tag{1}$$

Buoyancy is defined as

$$F_b = \rho V g = \rho\frac{\pi}{3}R^3 f(\theta) g \tag{2}$$

where $\rho = 10^3$ kg/m^3 is the density of the liquid (water), V is the bubble volume (m^3), $g = 9.8\ m/s^2$ is the acceleration due to gravity, and $f(\theta) = 2 + 3\cos\theta - \cos^3\theta$ is a geometrical factor describing the dependence of the bubble volume on the contact angle for a fixed radius of curvature.[26]

We will consider a bubble with radius of curvature $R = 30\ \mu$m on extended planar surfaces with contact angles of 120° and 60°, which are close to our measured values of 120° and 70°, respectively. The radius of the contact area stays the same for both cases, $a = a' = R\sin\theta = 26.0\ \mu$m; see Figure 1B. With the surface tension of water in contact with air at 20 °C (72.8 mN/m), we then obtain for both types of surfaces $F_c = 1.03 \times 10^{-5}$ N.

The wetting properties are contained in the geometric function $f(\theta)$ which assumes values of $f(120°) = 5/8$ and $f(60°) = 27/8$. Therefore, the buoyancy force differs by almost a factor of 6, because for fixed R the volumes are different. Inserting the values above, we obtain

$$F_b(120°) = 1.7 \times 10^{-10}\ \text{N and } F_b(60°) = 9.4 \times 10^{-10}\ \text{N}$$

F_b is several orders of magnitude smaller than F_c, and hence, buoyancy will not remove bubbles with $R < 30\ \mu$m from a hydrophilic surface; on a hydrophobic surface they will stick with even stronger force.

We may also consider the case that a bubble once formed on hydrophobic areas could move onto a hydrophilic area where it could stick because of capillary forces. If we now consider the force on different areas, we have to assume that the bubble will move with a constant volume, and on approach of a hydrophilic surface from a hydrophobic one it would change the contact area (Figure 1C). Thus, the radius of curvature, R, would be transformed into a smaller radius of curvature, R'. Volume conservation would yield $R^3 f(120°) = R'^3 f(60°)$. In the specific example, the radius would decrease by the third root of 27/5 = 1.8, and, according to eq 1, this would also hold for F_c. Hence the attraction to the hydrophobic surface is stronger, and once a bubble comes into contact with both types of surfaces, (e.g., during movement), it will be attracted toward the hydrophobic stripes. To conclude regarding the question of bubble attraction, bubbles would remain attached against buoyancy to both types of surfaces with broad stripes observed in this work. Therefore, it is deduced that preferential nucleation is responsible for the observed arrangement only on the hydrophobic surfaces, in addition to the lateral force moving attached bubbles from the hydrophilic regions. The latter phenomenon can be understood by the energy barrier from different capillary forces for bubbles of equal volume, as demonstrated above.

We now turn our attention to the narrower stripes. In this case confinement of the attachment of a bubble with fixed volume to one narrow hydrophobic stripe will reduce the contact area as well as the effective contact angle. For simplicity we assume that the free (spherical) bubble's radius remains constant at 30 μm but that the equivalent radius of the contact area is restricted to about 2 μm. F_c scales with $R\sin^2\theta$, where $R \approx 30\ \mu$m and $\sin\theta \approx a/R = 2/30$. With these values we obtain $F_c \approx 6 \times 10^{-8}$ N, while $F_b \approx 1 \times 10^{-9}$ N. If buoyancy exceeds the capillary force, for both types of surfaces we would assume that all large bubbles would leave the surface. However, as F_b scales with the third power of R, this crossover is expected around $R = 80\ \mu$m, and we should observe smaller bubbles on the surface. This value is much smaller than F_b for a hydrophobic surface, but $F_b \approx F_c$ for a hydrophilic surface. Hence smaller bubbles should stick on narrow hydrophobic stripes, and the question of why we do not observe them arises. One reason may be that the bubbles require gas adsorption on a hydrophobic surface, and there is not enough gas available for bubble nucleation and growth. We assume that the latter is dominant with the following rough estimate: A typical gas molecule number density on a hydrophobic surface is around 10^6 per μm^2 and the gas density in a bubble at 1 atm pressure is 2.7×10^7 per μm^3. Hence, a surface area of 1 μm^2 delivers enough gas molecules to fill a nucleus of $R = 0.1\ \mu$m. However, it does not deliver enough molecules to fill a bubble that will grow beyond a few micrometers. Nevertheless, it is also possible that there is nucleation, but the nuclei are optically not observable. A second reason may be that growing bubbles become asymmetric, and this inhibits growth or makes them unstable.

Finally, we discuss the role of the Bjerknes forces, F_{Bj}. This results from a correlation of time varying bubble volume $V(t)$ and oscillating acoustic pressure gradient $\nabla p_a(t)$ at the bubble's position, according to a nonvanishing time average $F_{Bj} = \langle V(t)\nabla p_a(t)\rangle$.[27] In our experiment, the water in the cylindrical Petri dish cell has a filling height of roughly half an acoustic wavelength at 86 kHz (8.6 mm) and a diameter of 60 mm. Direct pressure measurements were not feasible, but we assume that an approximate standing wave field developed in the cell in which the very small bubbles (below linear resonance radius) are driven to the pressure antinodes.[27] This is considered as the reason why some bubbles from the bulk were observed to be moving to the substrate where they finally attach. An estimation of magnitude

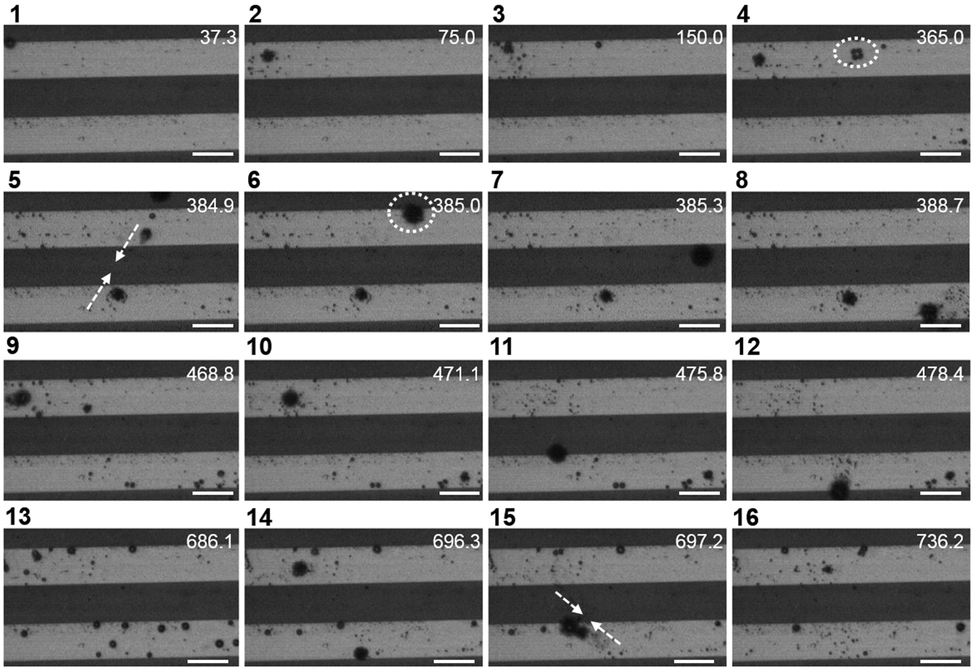

Figure 4. Selected frames from a high-speed sequence taken at 100 000 fps with microscope magnification of ×10. The numbers in the top right corners of the frames indicate the elapsed time in milliseconds after the start of acoustic irradiation. The scale bar is 100 μm. The width of the hydrophobic (bright) stripes is 82 μm; the width of the hydrophilic (dark) stripes is 90 μm. This movie is available in the Supporting Information (Movie S1).

of the primary (sound-field-induced) Bjerknes force for the assumption of small linear pulsations in a plane ultrasonic standing wave field of 86 kHz and an amplitude of 50 kPa leads to a maximum value of about 6×10^{-7} N for a bubble of equilibrium radius $R_0 = 30$ μm (see the Appendix for details). This is enough to overcome gravity effects (10^{-9} N) but is smaller than the estimated capillary attachment force of about 10^{-5} N.

The attachment process is supported by a type of secondary Bjerknes force. These forces originate from the pressure waves emitted by neighboring bubbles and result in mutual attraction of bubbles of similar size.[27−29] In our experiment, the (single) bubble's own emitted pressure waves are reflected from the solid substrate which leads to a force toward the substrate, according to a virtual "mirror bubble" on the other side of the sound-hard boundary.[30,31] This phenomenon is well-known and documented for approaching bubbles,[32] but the force strength for already attached oscillating bubbles is not straightforward. In particular, the bubble dynamics becomes nonspherical and potentially complicated at short distances from the boundary.[33−35] Therefore, we only give a quantitative estimation for spherical bubbles approaching the solid from the bulk but not being in direct contact with the substrate; see the Appendix. This shows, for instance, that our reference bubble of equilibrium radius $R_0 = 30$ μm at 86 kHz and a radial pulsation of 20% should feel an attractive force of 10^{-5} N when 70 μm away from a perfectly reflecting (i.e., sound-hard) surface. This is already the order of the capillary attachment forces, and it should be exceeded at even closer distances.

We conclude that primary Bjerknes forces are responsible for the motion of bubbles in the bulk liquid and for guiding some of them toward the substrate but that they play only a negligible role in determining the attachment strength. The approach of bubbles is further supported by the "mirror bubble" effect due to secondary Bjerknes forces. However, while the contribution of this effect to the attachment strength is undoubted, its exact values and the dependence on the hydrophobicity, i.e., its variation for the different stripes, remain unclear. In any case, this cannot remove bubbles from a surface.

Both Bjerknes forces apparently play a role in the migration process of bubbles on the surface. Horizontal components of the primary Bjerknes force as well as attraction or repulsion between closely (horizontally) spaced bubbles may be the drivers for their motion along the stripes, their separation after splitting, and their mutual approach and merging. These aspects are shown in more detail below.

To better understand the relationship between the size of the hydrophobic area and the bubbles' behavior, a higher microscope magnification (×10) was used to monitor surface bubble growth. Figures 4 and 5 show cavitation recorded on the sample area with hydrophobic stripes of 82 and 57 μm width, respectively. The samples were not enriched with gas as was done in the example described above; therefore, surface cavitation was not as intense as for the preconditioned samples. Wet etching was used to enhance the visual contrast of the stripes. Under optical microscopy, hydrophilic stripes now appear dark and hydrophobic stripes pale because of light interference. The frames in Figure 4 show that surface cavitation is an extremely chaotic process, although the bubbles are constrained to the hydrophobic areas. It is important to note that bulk bubbles are involved in the surface cavitation process. Supporting Information Movie S1 demonstrates clearly how the bulk bubble impacts the hydrophobic stripe at 37.3 ms and initiates surface cavitation (Figure 4, frame 1). It is likely that this bubble formed outside the bulk area captured by the camera. This initial bubble is henceforth referred to as a "mother bubble" generating smaller bubbles ("daughter bubbles") which reside only within the hydrophobic stripes (frames 2, 3). Newly formed bubbles are partially absorbed by the initial mother bubble, whereas others keep moving along the hydrophobic stripes.

Further analyzing the recording, several points warrant attention: (i) new surface bubbles come from the bulk or existing attached bubbles; (ii) the bubbles move laterally as they

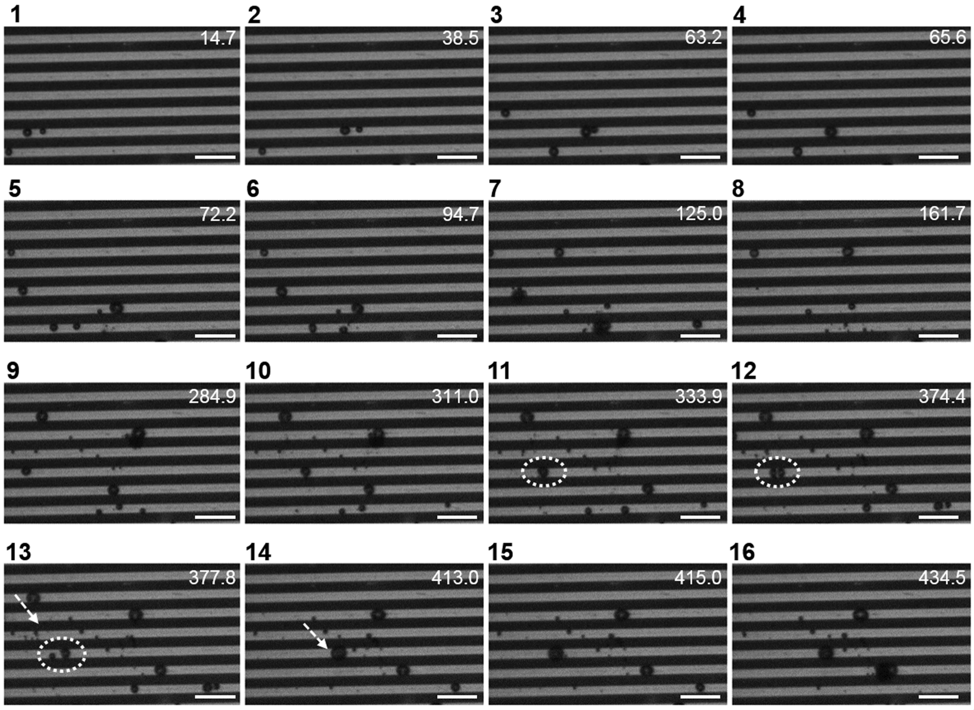

Figure 5. Selected frames from a high-speed sequence taken at 100 000 fps with microscope magnification of ×10. The numbers in the top right corners of the frames indicate the elapsed time in milliseconds after the start of acoustic irradiation. The scale bar is 240 μm. The width of the hydrophobic (bright) stripes is 57 μm; the width of the hydrophilic (dark) stripes is 60 μm. This movie is available in the Supporting Information (Movie S1).

reach a certain size (roughly above 10 μm); (iii) they grow by traveling or collecting other small bubbles; (iv) they can merge and form agglomerates on the same stripe (frames 4, 6); (v) they can travel toward each other (frame 5, 15); and (vi) they can split into smaller bubbles, which partially reside within the same hydrophobic stripe or move to the next hydrophobic stripe (frames 3, 11, 12). Additionally, bubbles do not grow beyond the width of the stripes, and the maximum detected size of a single bubble attached to the surface is about 1/3 of the stripe width. After the bubbles reach their maximum size they move away from the substrate into the bulk.

The observation of cavitation on the sample with 57-μm wide hydrophobic stripes (Figure 5, Movie S1 in the Supporting Information) indicates that the bubble behavior changes from chaotic to ordered. However, the interactions between bubbles and bubble—surface are similar to those discussed above. We observe that the bubbles are attached to the hydrophobic—hydrophilic boundaries which also restrict bubble growth and their movement within the hydrophobic stripes. In our observations, the bubbles do not exceed the 57-μm stripe width. Individual bubbles, which travel laterally on the surface, can be followed and studied in detail. The shape of individually traveling bubbles is spherical. By tracking the movement of a single bubble in Figure 5, it is possible to determine its velocity. For example, the bubbles running from frames 1 to 2 move at an average velocity of 0.018 ms^{-1} with a peak velocity of 0.3 ms^{-1}. The bubble moving back and forward in frame 14 reaches a peak velocity of around 0.25 ms^{-1}; the bubbles that can be seen jumping from one stripe to another (indicated by a white arrow, frames 13—14) also reach velocities of 0.25—0.15 ms^{-1}. Additionally, on this patterned region it is easy to track splitting and multiplication of bubbles. After splitting, bubbles undergo asymmetric deformation of their walls and show jet formation toward each other (this bubble transformation is marked by a white dashed circle in frames 11 and 12). The split-off bubbles do not all have the same volume (frame 13).

The nature of the surface as well as its dimensions influence the dynamics of the three-phase line and bubble growth. This is confirmed by a similar observation under the same ultrasonic conditions on the patterned region with smaller hydrophobic stripes, in which case the bubbles were restricted to the stripe width of 23 μm (Supporting Information Figure S1, Movie S2). In this video, bubbles propagate laterally mostly in one direction, from the right side of the bulk area captured by the camera to the left. With an interval of a few milliseconds of ultrasonic irradiation the bubbles come close to each other, and some of them merge into larger bubbles. Eventually the bubbles become large enough and leave the stripes. The remaining bubbles split into new small bubbles and continue to propagate within the stripes. After 0.03 s of ultrasonic irradiation (Supporting Information Figure S1, frame 7), all hydrophobic stripes are covered by attached cavitation bubbles.

It is reasonable to assume that the driving forces for bubble movement are the acoustic (Bjerknes) forces as discussed above. The reason for confinement to the hydrophobic areas might be a capillary energy barrier for attachment, gas species, which may be present on the surface due to selective adsorption of dissolved gas from the liquid[20,22] or the adsorption of fragments from collapsing cavitation bubbles. Furthermore, all above-discussed results clearly demonstrate that the bubbles undergo shape changes caused by their splitting or multiplying on the substrate. Further research has to be undertaken to visualize the cavitation events from the side view on the patterned surface to better understand selective bubble growth and bubble movement at surfaces with varying surface energy.

CONCLUSIONS

We designed and carried out a novel set of experiments to monitor surface cavitation at chemically well-defined, structured patterns with alternating hydrophobic and hydrophilic surface regions. The size of the hydrophobic stripes ranged from 3.5 to 115 μm. Using a top-view technique, we clearly saw that the bubbles strongly avoid hydrophilic areas. Although it was possible to observe some small bubbles located on the hydrophilic stripes, these remained unchanged under ultrasonic irradiation. The experimental results revealed good agreement with the theoretical predictions. The behavior of cavitation bubbles was discussed by estimating the forces acting on a bubble near a surface. The buoyancy force and a potential repulsion from the solid surface due to primary Bjerknes forces are too small to remove bubbles from the surface for the dimensions relevant in this work (i.e., <100 μm). On the other hand, secondary Bjerknes forces (via "the mirror bubble effect") seem to contribute to the approach and the attachment of bubbles from the bulk liquid, but the strength of the forces for already attached bubbles and their dependence on the contact angle, and thus their influence on the surface selectivity, remain unknown. Our estimates based on the other forces quantify the stronger attachment of bubbles of the same volume to hydrophobic surfaces. The existence of a lower stripe width for the observation of attached bubbles can be ascribed to the limited growth from surface adsorbed gas. Although this may be specific to our system, it may also provide a way to control cavitation via surface structuring and may be relevant for bubble growth on confined surfaces, such as on microparticles. This work provides a significant contribution to the investigation of acoustic erosion on solid surfaces with the aim to predict cavitation and to fabricate new erosion-resistant coatings. Additionally, this study advances the application of ultrasound for the controllable fabrication of well-designed materials with defined physical or chemical properties which can be used in physical and colloidal chemistry and biology or for medical purposes.

METHODS

Scanning electron microscopy (SEM) investigations were performed using a Gemini Leo 1550 microscope at an operating voltage of 3 keV. To reduce sample charging and to increase the thermal conduction, a 3–5 nm gold layer was sputtered on the patterns before each set of measurements.

Atomic force microscopy (AFM) investigations were performed using a Nanoscope III Multimode AFM (Digital Instruments Inc., U.S.A.) operating in tapping mode with a monolithic Silicone probe. The consistent tip radius of less than 15 nm allowed us to determine roughness and height of the hydrophobic areas with a good resolution and reproducibility.

A contact angle meter (Software DSA 1, Kruess GmbH) was used to measure the contact angle (CA) of patterned samples. Since one field of the patterns is in the range of 2 × 2 mm^2, the CA measurements were performed at room temperature on samples with equal structure but larger dimensions (10 × 10 mm^2). Deionized Milli-Q water droplets (3 mL) were placed on the surfaces, and the advancing CAs were measured at three different positions for each sample.

The software ImageJ was used to improve the quality of the pictures and videos. ImageJ is a widely used Open Source software employing image analysis and quality control in the graphic arts technologies (released under the GPL license).[36]

APPENDIX

We approximate the sound pressure field in the Petri dish above the substrate by a plane wave in the vertical (z) direction,

$$p_a(z, t) = A\cos(kz)\cos(\omega t)$$

with sound pressure amplitude A, acoustic wavenumber $k = \omega/c$, acoustic frequency f, angular frequency $\omega = 2\pi f$, and sound speed in water c. The primary Bjerknes force on an oscillating bubble of equilibrium radius R_0 and radial oscillation amplitude ΔR is calculated via

$$F_{Bj1} = -\langle \nabla p_a(z, t) V(t)\rangle$$

where $\langle . \rangle$ denotes time average. The time varying bubble volume $V(t)$ is supposed to follow the period of the driving pressure, and for $\Delta R/R_0$ small enough we can employ a linear approximation:

$$V(t) = \frac{4\pi}{3}{R_0}^3 - 4\pi {R_0}^2 \Delta R\cos(\omega t + \phi)$$

To estimate the maximum force, we set $\phi = 0, \pi$ (i.e., pure in-phase or antiphase oscillations in relation to the sound pressure), and assume a bubble position with $\sin(kz) = \pm 1$ (i.e., maximum pressure gradient). This leads to

$$|F_{Bj1}|_{\max} = |\langle \pm 4\pi k A R_0^2 \Delta R\cos^2(\omega t)\rangle| = 2\pi k A {R_0}^2 \Delta R = \frac{4\pi^2 f}{c} A {R_0}^2 \Delta R$$

With $f = 86$ kHz, $c = 1482$ m/s, $A = 5 \times 10^4$ Pa, $R_0 = 30\ \mu$m, and an oscillation strength of $\Delta R/R_0 = 0.2$, we obtain $|F_{Bj1}|_{\max} \approx 6 \times 10^{-7}$ N. This estimate shows that at moderate sound pressures the primary Bjerknes forces can easily overcome buoyancy effects but not capillary attachment forces. Lateral drift of attached bubbles on the substrate, however, might well be caused by primary Bjerknes forces if horizontal sound pressure field gradients exist.

The secondary Bjerknes force is the mutual attraction or repulsion force of closely neighboring oscillating bubbles. For spherical bubbles with not too small distance d between their centers, we can use the approximation (ref 28)

$$F_{Bj2} = -\frac{\rho}{4\pi d^2}\left\langle \frac{\mathrm{d}}{\mathrm{d}t}V_1(t)\frac{\mathrm{d}}{\mathrm{d}t}V_2(t)\right\rangle$$

for the force of bubble "1" on bubble "2". Here, ρ is the liquid density, the force acts in the direction of the distance vector, and negative values represent attraction. For the case of the "mirror bubble effect", the respective bubble volumes are equal, $V_1(t) = V_2(t) = V(t)$, the distance of the bubble center to the substrate is $h = d/2$, and the force direction is always toward the solid boundary which is supposed to reflect the sound waves perfectly. When employing a similar linear approximation of the bubble oscillation as above, we find

$$\frac{\mathrm{d}}{\mathrm{d}t}V(t) = \pm 4\pi\omega {R_0}^2 \Delta R\sin(\omega t)$$

which results in the estimate

$$|F_{Bj2}| = \frac{\rho}{4\pi(2h)^2}|\langle [4\pi(2\pi f){R_0}^2 \Delta R\sin(\omega t)]^2\rangle| = \frac{8\pi^3 \rho f^2}{h^2}{R_0}^4 \Delta R^2$$

This expression diverges as the bubble approaches the boundary, i.e., for $h \to 0$, and the range of validity of the approximation above is limited to a finite h of the order of at least several R_0.[34] For closer approach of the bubble to the substrate, multiple scattering,[37] bubble deformations, and other effects like contact angle upon direct attachment[38] have to be taken into account. However, we are not aware of published results immediately applicable to the problem of the attachment force of an oscillating nonspherical bubble, and thus we only estimate the attraction of spherical bubbles from the bulk liquid at some closer distance employing the above formula. With ρ = 1000 kg/m^3, $\Delta R/R_0 = 0.2$, and other values as above, the bubble of $R_0 = 30$ μm feels an attractive force of $|F_{Bj2}|_{\max}$ 6 × 10^{-7} N at a distance of $h = 10R_0$, a force comparable to the capillary attachment force of 10^{-5} N at $h \approx 70$ μm, and a force larger than 5 × 10^{-5} N for an approach close to its own size, $h = R_0$. Of course, these values have to be modified if a more accurate model is considered, but we expect that the order of magnitude persists. On the other hand, larger deviations of these values are to be expected for variations of bubble size and oscillation amplitude, which deserves a separate study. In any case, the estimation shows that the secondary Bjerknes effect can contribute substantially to the attachment strength of bubbles to a solid substrate. However, as this force scales with R_0^4 it may only hold for large enough bubbles.

■ ASSOCIATED CONTENT

Ⓢ Supporting Information

Figure S1 showing selected frames of surface cavitation on pattern area with hydrophobic stripes of 23 μm width and Movies S1 and S2 showing surface cavitation recorded with a high speed camera. This material is available free of charge via the Internet at http://pubs.acs.org.

■ AUTHOR INFORMATION

Corresponding Authors

*V.B.-M. E-mail: valentina.belova@mpikg.mpg.de.
*R.M. E-mail: robert.mettin@phys.uni-goettingen.de.

Author Contributions

The manuscript was written through contributions of all authors. All authors have given approval to the final version of the manuscript. All authors contributed equally.

Notes

The authors declare no competing financial interest.

■ ACKNOWLEDGMENTS

The authors acknowledge the Max Planck Society for the financial support. A.B. acknowledges receipt of an Alexander von Humboldt fellowship. The support of C.C. and R.M. by the Austrian Federal Ministry of Economy, Family and Youth is gratefully acknowledged. We thank A. A. Doinikov for helpful comments. The authors would like to thank Karin Ahlborn from the Institute of Materials Physics, Georg-August-University Göttingen, for loan of the microscope.

■ REFERENCES

(1) Rayleigh, L. On the Pressure Developed in a Liquid during the Collapse of a Spherical Cavity. *Philos. Mag.* **1917**, *34*, 94−98.

(2) Suslick, K. S.; Crum, L. A. *Sonochemistry and Sonoluminescence, in Encyclopedia of Acoustics*; Crocker, M. J., Ed.; Wiley-Interscience, New York, 1998; pp 243−253.

(3) Rae, J.; Ashokkumar, M.; Eulaerts, O.; von Sonntag, C.; Reisse, J.; Grieser, F. Estimation of Ultrasound Induced Cavitation Bubble Temperatures in Aqueous Solutions. *Ultrason. Sonochem.* **2005**, *12*, 325−329.

(4) Mason, T. J.; Lorimer, J. P. *Sonochemistry: Theory, Applications and Uses of Ultrasound in Chemistry*; Ellis Horwood: Chichester, U.K., 1988.

(5) Westwater, J. W. *Boiling of liquids*; Advances in Chemical Engineering; Academic Press: New York, 1956; Vol. *1*, Ch. 1.

(6) Thiruvengadam, T.; Waring, S. Mechanical Properties of Metals and their Cavitation Damage Resistance. *J. Ship Res.* **1966**, *10*, 1−9.

(7) Cabrera, E.; Espert, V.; Martinez, F. *Hydraulic Machinery and Cavitation*; Kluwer Academic Publisher: Dordrecht, The Netherlands, 1996; Vol. 2, pp 905−914.

(8) Hammitt, F. G.; De, M. K. Cavitation Erosion of Aluminum considering Bubble Collapse, Pulse Height Spectra and Cavitation Erosion Efficiency. *Wear* **1979**, *55*, 221−234.

(9) Suslick, K. S.; Flannigan, D. J. Inside a Collapsing Bubble: Sonoluminescence and the Conditions during Cavitation. *Annu. Rev. Phys. Chem.* **2008**, *59*, 659−683.

(10) Xiong, H.-M.; Shchukin, D. G.; Möhwald, H.; Xu, Y.; Xia, Y.-Y. Sonochemical Synthesis of Highly Luminescent Zinc Oxide Nanoparticles Doped with Magnesium (II). *Angew. Chem.* **2009**, *121*, 2765−2769.

(11) Lauterborn, W.; Kurz, T.; Mettin, R.; Ohl, C. D. Experimental and Theoretical Bubble Dynamics. Advances in Chemical Physics. *Adv. Chem. Phys.* **1999**, *110*, 295−380.

(12) Ohl, C.-D.; Kurz, T.; Geisler, R.; Lindau, O.; Lauterborn, W. Bubble Dynamics, Shock Waves and Sonoluminescence. *Philos. Trans. R. Soc., London Ser. A* **1999**, *357*, 269−294.

(13) Lindau, O.; Lauterborn, W. Cinematic Observation of the Collapse and Rebound of a Laser-produced Cavitation Bubble near a Wall. *J. Fluid Mech.* **2003**, *479*, 327−348.

(14) Krefting, D.; Mettin, R.; Lauterborn, W. High-speed Observation of Acoustic Cavitation Erosion in Multibubble System. *Ultrason. Sonochem.* **2004**, *11*, 119−123.

(15) Bremond, N.; Arora, M.; Ohl, C.-D.; Lohse, D. Controlled Multibubble Surface Cavitation. *Phys. Rev. Lett.* **2006**, *96*, 224501−4.

(16) Belova, V.; Gorin, D. A.; Shchukin, D. G.; Möhwald, H. Controlled Effect of Ultrasonic Cavitation on Hydrophobic/Hydrophilic Surfaces. *ACS Appl. Mater. Interfaces* **2011**, *3*, 417−425.

(17) Skorb, E. V.; Andreeva, D. V. Surface Nanoarchitecture for Bio-Applications: Self-regulated Intelligent Surfaces. *Adv. Funct. Mater.* **2013**, *23*, 4483−4506.

(18) Anselme, K.; Noel, B.; Hardouin, L. L. Human Osteoblast Adhesion on Titanium Alloy, Stainless Steel, Glass and Plastic Substrates with same Surface Topography. *J. Mater. Sci. Mater. Med.* **1999**, *10*, 815−819.

(19) Burdinski, D.; Saalmink, M.; van den Berg, J. P. W. G.; van der Marel, C. Universal Ink for Microcontact Printing. *Angew. Chem., Int. Ed.* **2006**, *45*, 4355−4358.

(20) Belova, V.; Krasowska, M.; Wang, D.; Ralston, J.; Shchukin, D. G.; Möhwald, H. Influence of Adsorbed Gas at Liquid/Solid Interfaces on Heterogeneous Cavitation. *Chem. Sci.* **2013**, *4*, 248−256.

(21) Phelps, A. D.; Leighton, T. G. The Subharmonic Oscillations and Combination-Frequency Emissions from a Resonant Bubble: their Properties and Generation Mechanisms. *Acta Acust.* **1997**, *83*, 59−66.

(22) Zhang, X. H.; Maeda, N.; Craig, V. S. J. Physical Properties of Nanobubbles on Hydrophobic Surfaces in Water and Aqueous Solutions. *Langmuir* **2006**, *22*, 5025−5035.

(23) Zhang, X. H.; Quinn, A.; Ducker, W. A. Nanobubbles at the Interface between Water and a Hydrophobic Solid. *Langmuir* **2008**, *24*, 4756−4764.

(24) Brotchie, A.; Zhang, X. H. Response of Interfacial Nanobubbles to Ultrasound Irradiation. *Soft Matter* **2011**, *7*, 265−269.

(25) Jones, S. F.; Evans, G. M.; Galván, K. P. Bubble Nucleation from Gas Cavities - a Review. *Adv. Colloid Interface Sci.* **1999**, *80*, 27−50.

(26) Blander, M.; Katz, J. L. Bubble Nucleation in Liquids. *AlChE J.* **1975**, *21*, 833−848.

(27) Leighton, T. G. *The Acoustic Bubble*; Academic Press, London, 1997.

(28) Mettin, R.; Akhatov, I.; Parlitz, U.; Ohl, C. D.; Lauterborn, W. Bjerknes Forces between Small Cavitation Bubbles in a Strong Acoustic Field. *Phys. Rev. E* **1997**, *56*, 2924−2931.

(29) Mettin, R. In *Bubble and Particle Dynamics in Acoustic Fields: Modern Trends and Applications*; Doinikov, A. A., Ed.; Research Signpost: Kerala, 2005; pp 1−36.

(30) Blake, J. R.; Taib, B. B.; Doherty, G. Transient Cavities near Boundaries. Part I. Rigid boundary. *J. Fluid Mech.* **1986**, *170*, 479−497.

(31) Sato, K.; Tomita, Y.; Shima, A. Numerical-Analysis of a Gas Bubble near a Rigid Boundary in an Oscillatory Pressure Field. *J. Acoust. Soc. Am.* **1994**, *95*, 2416−2424.

(32) Xi, X.; Cegla, F.; Mettin, R.; Holsteyns, F.; Lippert, A. Collective Bubble Dynamics near a Surface in a Weak Acoustic Standing Wave Field. *J. Acoust. Soc. Am.* **2012**, *132*, 37−47.

(33) Pelekasis, N.; Tsamopoulos, J. Equilibrium Shapes and Stability of an Oscillatory Pressure Field. *J. Fluid Mech.* **1993**, *254*, 501−527.

(34) Doinikov, A. A. Acoustic Radiation, Interparticle Forces in a Compressible Fluid. *J. Fluid Mech.* **2001**, *444*, 1−21.

(35) Marmottant, P.; Versluis, M.; de Jong, N.; Hilgenfeldt, S.; Lohse, D. High-speed Imaging of an Ultrasound-driven Bubble in Contact with a Wall: "Narcissus" Effect and Resolved Acoustic Steaming. *Exp. Fluids* **2006**, *41*, 147−153.

(36) ImageJ RSB Home page. http://imagej.nih.gov/ij/ (accessed June 19, 2014).

(37) Harkin, A.; Kaper, T. J.; Nadim, A. Coupled Pulsation and Translation of Two Gas Bubbles in a Liquid. *J. Fluid Mech.* **2001**, *445*, 377−411.

(38) Maksimov, A. O. On the Volume Oscillations of a Tethered Bubble. *J. Sound Vib.* **2005**, *283*, 915−926.